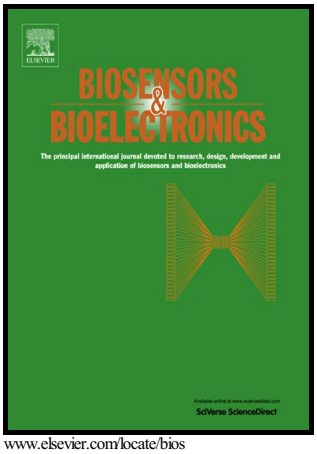

www.elsevier.com/locate/bios

Near-infrared fluorescence nanoprobe for enzyme-substrate system sensing and *in vitro* imaging

Xu Yan, Tianyu Hu, Lei Wang, Lening Zhang, Xingguang Su

PII: S0956-5663(16)30001-X
DOI: http://dx.doi.org/10.1016/j.bios.2016.01.001
Reference: BIOS8341

To appear in: *Biosensors and Bioelectronic*

Received date: 1 October 2015
Revised date: 21 December 2015
Accepted date: 2 January 2016

Cite this article as: Xu Yan, Tianyu Hu, Lei Wang, Lening Zhang and Xingguang Su, **Near-infrared fluorescence nanoprobe for enzyme-substrate system sensing and *in vitro* imaging**, *Biosensors and Bioelectronic* http://dx.doi.org/10.1016/j.bios.2016.01.001

Near-infrared fluorescence nanoprobe for enzyme-substrate system sensing and *in vitro* imaging

Xu Yan,[a] Tianyu Hu,[a] Lei Wang,[a] Lening Zhang,[b] and Xingguang Su[a,*]

[a] *Department of Analytical Chemistry, College of Chemistry, Jilin University, Changchun, 130012, China*

[b] *Department of Thoracic Surgery; China-Japan Union Hospital of Jilin University, Changchun, 130033, China*

*Corresponding author

Tel.: +86-431-85168352

E-mail address: suxg@jlu.edu.cn

ABSTRACT

Herein we report a simple and sensitive fluorescent sensing platform for phenol and enzyme activity detection based on 3-aminobenzeneboronic acid functionalized $CuInS_2$ QDs (APBA-$CuInS_2$ QDs). APBA were covalently linked to $CuInS_2$ QDs surface to form the APBA-$CuInS_2$ QDs which had a fairly symmetric fluorescence emission peak at 736 nm in the near-infrared spectral region. In the presence of tyrosinase, phenol can be catalyzed the oxidization into catechol, which could reactive toward the boronic acid functional groups of APBA-$CuInS_2$ QDs to form five-membered cyclic esters, leading to the fluorescence quenching of the QDs. The effective fluorescence quenching of APBA-$CuInS_2$ QDs by phenol enabled this proposed nanosensor to sensitively detect the phenol product-related enzyme system, such as acid phosphatase-catalyzed hydrolysis of phenyl phosphate. Thus, the proposed biosensor was utilized for facile, sensitive, and selective detection phenol, tyrosinase and acid phosphatase. The detection limits of phenol, tyrosinase and acid phosphatase reached 0.05 μmol L^{-1}, 0.03 $U \cdot mL^{-1}$ and 6 $nU \cdot mL^{-1}$ for, respectively. The feasibility of the proposed nanosensor in real samples assay was also studied and satisfactory results were obtained. Meanwhile, using the APBA-$CuInS_2$ QDs fluorescence probe, we successfully performed *in vitro* imaging of human prostate cancer cells, suggesting the biocompatible sensor has potentially extensive application clinic diagnoses assays.

Key words: Near-infrared biosensor; phenol; acid phosphatase; tyrosinase; *in vitro* imaging

1. Introduction

Semiconductor quantum dots (QDs) have been receiving much research interest during the past few decades due to their great potential applications in imaging, diagnosis and optoelectronic devices (Gill et al., 2013; Chen et al., 2013; Freeman et al., 2013). The high quantum yields, broad excitation bands and pronounced photostability in comparison with organic dyes, also make them highly promising nanomaterials for the construction of various chemical and biological sensing platforms (Wu et al., 2013; Morris-Cohen et al., 2013; Li et al., 2013). Moreover, they are highly resistant to photobleaching and have relatively large surface area for bio/chem modification (Medintz et al., 2005). However, in the development of semiconductor nanocrystals, traditional semiconductor usually containing toxic materials, such as cadmium, mercury and lead, that have strong cytotoxic activity and eventually would cause serious environmental problems (Derfus et al., 2004; Kirchner et al., 2005; Pradhan et al., 2007). As newly generation of QDs, ternary $CuInS_2$ QDs have attracted considerable interests in sensing, delivering drugs and bio-imaging applications recently (Liu et al., 2013; Lin et al., 2014). This is not only due to their negligible cytotoxicity and environmental friendliness but also due to their unique chemical and physical properties, such as larger Stokes shifts (Liu et al., 2014). Most importantly, the $CuInS_2$ QDs have a fluorescence emission peak in the near-infrared (NIR) spectral region. The NIR fluorescence signal can avoid interferences from biological media because the NIR wavelength (650–900 nm) light has strong tissue penetration, low tissue scattering effects and induces minimal autofluorescence (Yong et al., 2009; Xia et al., 2011; Van Veggel et al., 2013). Hence, these attractive superiorities of $CuInS_2$ QDs result in potentiating them as ideal chem/bio sensor and bio-imaging platforms.

Enzymes known as nature's catalysts provide the critical means by which to efficiently catalyze almost all biochemical processes in a controlled manner and precise specificity. This has made enzymes of considerable interest for utilizing in the construction of biosensors. Recently, enzyme-based biosensors, as an alternative to the conventional analytical methods, have been generally considered as simple and sensitive technique for selectively detecting target analyte (Van Dyk et al., 2011; Azmi et al., 2015). Combinations of QDs and enzyme molecules have exhibited great prospects for health-care monitoring, environmental applications, food safety and agricultural practices, since both the unique structural and photophysical performance and excellent specificity have been effectively integrated (Gill et al., 2006; Gao et al., 2012; Akshath et al., 2014; Yan et al., 2015a). For example, Yan et al designed a sensitive and reliable dual-emission ratiometric fluorescence probe, which shows dual-emission for the visual observation of tyrosinase activity (Yan et al., 2015b). Breger et al describe a highly sensitive QD-peptide nanosensor for monitoring the activity of kallikrein on the basis of förster resonance energy transfer (Breger et al., 2014). Serrano et al present two color encoded silica nanospheres for the fluorescence quantitative ratiometric determination of trypsin in humans (Serrano et al., 2014). Tang's group developed a simple and sensitive method for determination of organophosphorus pesticides in real samples based on acetylcholinesterase and choline oxidase (Meng et al., 2013). This indicates that enzyme-based biosensors with QDs have become a research hotspot, especially bi-enzyme sensing platforms. The QDs based bi-enzyme system has the advantages of multi-signal amplification and simple detection procedure without the need of enzyme immobilization, and also can detect analytes optically.

Recently, our group integrated 3-aminobenzeneboronic acid functionalized $CuInS_2$ QDs

(APBA-$CuInS_2$ QDs) to realize convenient and real-time assays for dopamine detection through the interaction between boronic acid and vicinal diols (Liu et al., 2013). On the basis of the preceding work, by combining the boronic acid-assisted target recognition and the specificity of enzyme, we herein ingeniously designed a novel optical bi-enzyme biosensor platform for the highly accurate detection of enzyme activity and its substrate (acid phosphatase, as a model) **(Scheme 1)**. APBA was covalently linked to the mercaptopropionic acid-capped $CuInS_2$ QDs, which had a fairly symmetric fluorescence emission centered at 736 nm in the NIR region. Acid phosphatase (ACP) can catalyze hydrolysis of phenyl phosphate to phenol under acidic condition. In the presence of tyrosinase (TYR), phenol was further oxidized into catechol. The APBA-$CuInS_2$ QDs containing boronic acid functional groups were efficient covalent bonds with catechol to form five-membered cyclic esters, leading to the fluorescence quenching of the QDs. Accordingly, this developed sensing platform was facile and cost-effective as well as highly sensitive and selective, making it promising as a candidate for phenol and enzyme activity analysis. The integration of TYR-catalyzed catechol formation and boronic acid-assisted specific recognition not only improves the sensitivity and specificity of the biosensing platform but also provides a new way for probing other phenol product-related enzyme system. Moreover, intracellular detection of TYR activity using the biocompatible sensor was also conducted successfully, which provides great potential in practical application of TYR-associated disease monitoring and clinic diagnostics. To the best of our knowledge, this is the first example of the construction of a fluorescence sensing platform for phenol and enzyme activity detection based on highly efficient APBA-$CuInS_2$ QDs.

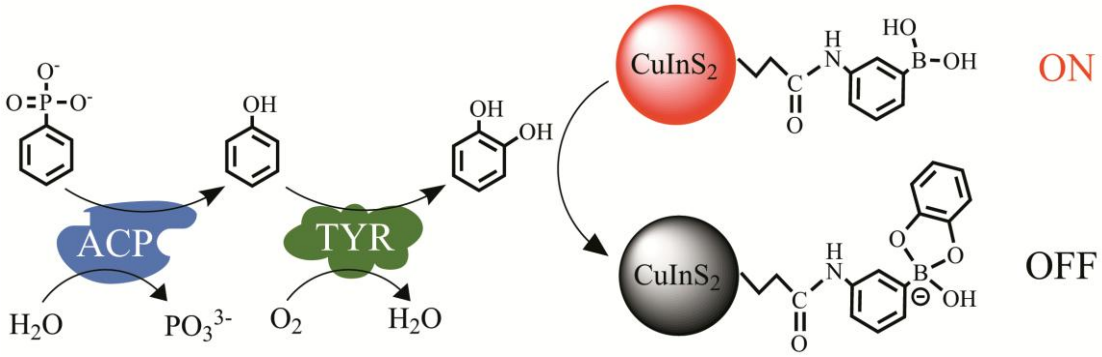

Scheme 1 The schematic illustration of the novel biosensor for phenol and enzyme activity detection based on 3-aminobenzeneboronic acid functionalized $CuInS_2$ QDs.

2. Experiment

2.1. Reagents and instruments

All reagents and solvents were of at least analytical grade. The water used in all experiments had a resistivity higher than 18 MΩ/cm. Copper (II) chloride dihydrate ($CuCl_2 \cdot 2H_2O$), sodium hydroxide (NaOH), sulfourea (CSN_2H_4), Tris(hydroxymethyl)aminomethane (Tris), Hydrogen chloride (HCl) and 1-ethyl-3-[3-dimethylaminopropyl] carbodiimide hydrochloride (EDC) were purchased from Beijing Chemical Works. Tyrosinase (TYR), 3-aminophenyl boronic acid (APBA), acid phosphatase (ACP), 3-Mercaptopropionic acid (MPA) and indium (III) chloride tetrahydrate ($InCl_3 \cdot 4H_2O$) were purchased from Sigma-Aldrich Corporation. Phenyl phosphate (PP) was obtained from Tianjin Guangfu Institute of elaborate chemical industry.

The fluorescence spectra were obtained by using a RF-5301 PC spectrofluorophotometer (Shimadzu, Japan) equipped with a xenon lamp using right-angle geometry. UV-Vis absorption spectra were recorded on a Cintra 10e UV-Vis spectrometer (GBC, Victoria, Australia). In both experiments, a 1 cm path-length quartz cuvette was used.

2.2. Preparation of 3-aminophenyl boronic acid-functionalized $CuInS_2$ QDs

$CuInS_2$ QDs were prepared in aqueous solution, according to our group previous report (Liu

et al., 2013). $CuCl_2 \cdot 2H_2O$ and $InCl_3 \cdot 4H_2O$ (0.15 mmol) were dissolved in 10.5 mL distilled water, and then 1.8 mmol MPA was dropped into the solution. After the mixture solution pH value was adjusted to 11.3, 0.30 mmol $CS(NH_2)_2$ was dissolved in the solution. The mixture solution was finally transferred into a 15 mL Teflon-lined stainless steel autoclave. Then it was heated and maintained at 150 ºC for 21 h and then cooled down to room temperature. The final concentration of $CuInS_2$ QDs was about 13.6 mmol L^{-1}.

The APBA-$CuInS_2$ QDs were synthesized according to previous report (Qu et al., 2013). The $CuInS_2$ QDs solution was mixed with EDC, and then APBA was added into the solution (the mole ratio of QD to EDC, APBA was 1:1500:500). The mixture was incubated for 3 h at room temperature and free of light. Finally, the resultant products APBA-$CuInS_2$ QDs were obtained.

2.3. Detection Procedure

100 μL purified APBA-$CuInS_2$ QDs solution were placed in a series of 2.0 mL calibrated test tubes. Subsequently, 80 μL TYR (500 U mL^{-1}) and different amounts of phenol were added, respectively. Then, the mixtures were diluted to 2.0 mL with pH 7.4 Tris-HCl (10 mmol L^{-1}) and mixed thoroughly at 37 ^{0}C. 60 min later, their fluorescence spectra were recorded in the 630–850 nm emission wavelength range at an excitation wavelength of 590 nm.

For the detection of TYR, different concentrations of TYR were mixed with 25 μmol L^{-1} phenol and 100 μL purified APBA-$CuInS_2$ QDs solution in a series of 2.0 mL calibrated test tubes. Then, the mixtures were diluted to 2.0 mL with pH 7.4 Tris-HCl (10 mmol L^{-1}). And fluorescence spectra were recorded after incubating at 37 ^{0}C for 60 min.

In our experiment, ACP was dissolved in 2.0 mmol L^{-1} Tris–HCl buffer solution (pH 6.0). 300 μL PP (250 μmol L^{-1}) and different amounts of ACP were mixed in a series of 2.0 mL

calibrated test tubes. 60 min later, 100 μL APBA-$CuInS_2$ QDs and 80 μL TYR (500 U mL^{-1}) were added into the above solutions. The mixtures were diluted to 2.0 mL with pH 7.4 Tris-HCl (10 mmol L^{-1}) and then mixed thoroughly and incubated for 60 min at 37 ^{0}C. At an excitation wavelength of 590 nm, the fluorescence spectra were recorded in the 630–850 nm emission wavelength range.

2.4. The in vitro imaging

Human prostate cancer cell line (PC-3M cells) was obtained as a gift from the college of medicine, Jilin University. The PC-3M cells were cultivated for 12 h in culture medium that contained IMDM supplemented with 10% fetal bovine serum at 37 ^{0}C. When the cultured cells reached about 70% confluence, the plates were washed with phosphate buffer saline (PBS) three times. Then, a certain amount of TYR was added to the PC-3M cell wells. After incubation for 3 h at 37 ^{0}C, free TYR was removed from TYR-uptaken PC-3M cells. Before in intracellular sensing experiments, IMDM medium was replaced by a fresh serum-free medium. The cells were incubated under the condition of serum starvation with APBA-$CuInS_2$ QDs/phenol for 60 min. Finally, fluorescent photos of the cells were obtained by an inverted fluorescence microscope equipped with a Nuance system.

3. Results and discussion

3.1. Characterization of the 3-aminobenzeneboronic acid functionalized $CuInS_2$ QDs

The APBA-$CuInS_2$ QDs were synthesized by covalently linking $CuInS_2$ QDs and APBA in the presence of EDC. As shown in **Fig. 1**, the formation of APBA-$CuInS_2$ QDs was characterized using the UV–vis spectroscopy, fluorescence spectroscopy, FT-IR spectroscopy and transmission electron microscopy (TEM). The UV–vis absorption spectra of $CuInS_2$ QDs, APBA and

APBA-$CuInS_2$ QDs were shown in **Fig. 1A**. There is no absorption band for APBA at 450–800 nm. The spectrum of $CuInS_2$ QDs showed a major characteristic absorption peak around 570 nm, while the absorption spectrum of the APBA-$CuInS_2$ QDs was shift to around 562 nm which different from that of $CuInS_2$ QDs. It maybe results from the effect of QDs surface functionalization. The fluorescence emission spectra of MPA-$CuInS_2$ QDs and APBA-$CuInS_2$ QDs are shown in **Fig. 1B.** It could be clearly observed that the fluorescence emission peak of $CuInS_2$ QDs had an significant red shift of 76 nm (from 660 nm to 736 nm) after the APBA were covalently linked to the surface of MPA-$CuInS_2$ QDs. This phenomenon was owing to the change of the surface functional groups from the negatively charged acetate to the strong electron-deficient boronic acid, resulting in the increase of the final $CuInS_2$ QDs size (Jin wt al., 2006; Tang et al., 2008; Liu et al., 2013). The FT-IR spectra of the MPA-capped $CuInS_2$ QDs and APBA-$CuInS_2$ QDs were shown in **Fig. 1C** to further demonstrate the formation of APBA-$CuInS_2$ QDs. As shown in **Fig. 1C** curve a, we can easily found the characteristic peaks of MPA (–COOH, 1575 cm^{-1} and 1420 cm^{-1}, $–CH_2$, 2925 cm^{-1} and 2850 cm^{-1}). After the covalent linking of $CuInS_2$ QDs and APBA, the peaks assigned to –COOH decreased or disappeared, while the peaks for amide groups (–CONH, 1560 cm^{-1}), phenyl ($–C_6H_4–$, 770 cm^{-1}, 795 cm^{-1}, 840 cm^{-1}), and C–N (2900 cm^{-1}) appeared and increased (**Fig. 1C** curve b). The majority of boronic acid functional groups could be clearly found through the characteristic peaks of B–O–H vibration (1340 cm^{-1}, 1240 cm^{-1} and 1095 cm^{-1}). These results further demonstrated that the $CuInS_2$ QDs were successfully functionalized by APBA. **Fig. 1D** shows the high resolution transmission electron microscopy (HRTEM) micrograph of APBA-$CuInS_2$ QDs. It can be seen that the size distribution of APBA-$CuInS_2$ QDs was reasonably uniform and the spherical particles size of was approximately 5 nm, showing clear lattice fringes

with a d spacing of 0.222 nm. Dynamic light scattering (DLS) experiments showed the average hydrodynamic diameter of fresh APBA-$CuInS_2$ QDs was about 26.7 nm (**Fig. S1**). These results indicate good water dispersibility and stability of APBA-$CuInS_2$ QDs.

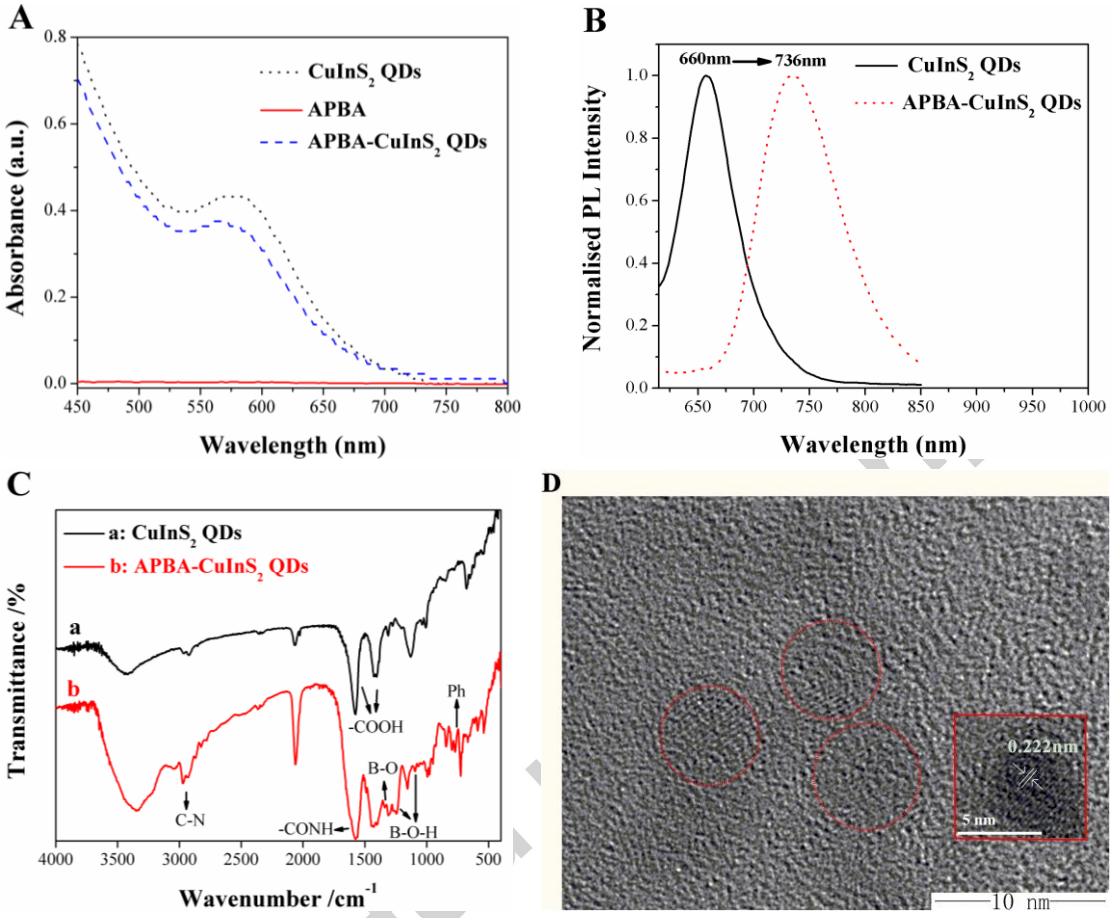

Fig. 1 (A) UV–vis spectra of pristine $CuInS_2$ QDs, APBA and APBA-$CuInS_2$ QDs; (B) The fluorescence emission spectra of $CuInS_2$ QDs (solid line) and APBA-$CuInS_2$ QDs (dash line); (C) The FT-IR spectra of the MPA-capped $CuInS_2$ QDs and ABPA-$CuInS_2$ QDs; (D) HRTEM images of APBA-$CuInS_2$ QDs nanoparticles.

3.2. Detection strategy of phenol and acid phosphatase

Towards building up a more sensitive method by quenching the fluorescence of ABPA-$CuInS_2$ QDs, we were trying to construct an enzyme system based on the oxidized activity

of TYR and the specific recognization of APBA. In the presence of TYR, phenol was oxidized into catechol, which could covalently combine with APBA functional groups to form stable five-membered cyclic boronate ester (**Scheme 1**). Thus, the fluorescence of the APBA-$CuInS_2$ QDs is quenched due to the formation of boronate complexes and the thickness increase of the surface capping layer of $CuInS_2$ QDs (Hoshino et al., 2004; Liu et al., 2013).

According to previous research, the boronic acid group could specifically reactive toward the vicinal diols to form boronate complexes (Wu et al., 2010; Tang et al., 2014). We demonstrated that the TYR/phenol reaction with APBA generated the boronate complexes by using UV–vis absorption (**Fig. S2)**. The spectrum of TYR showed a major characteristic absorption peak around 280 nm. In the presence of phenol, TYR could catalyze phenol to quinine, which appears a new absorption at 380 nm. When TYR, phenol and APBA existed together, the boronate complexes formed with two absorption peaks at 325 nm and 510 nm. In the view of the above, we confirmed that APBA could reactive toward catechol to form stable boronate complexes at the surface of $CuInS_2$ QDs.

The PL quenching of APBA-$CuInS_2$ QDs was considered to be related to the formation of boronate complexes. For better explanation of the mechanism, fluorescence lifetimes of APBA-$CuInS_2$ QDs were investigated. Fluorescence decay curves were illustrated in **Fig. S3**, and the fitting results of decay time were listed in **Table S1**. The APBA-$CuInS_2$ QDs had three components including 0.43 ns (38.49%), 5.04 ns (28.16%), and 62.27 ns (33.35%), and the average lifetime was 22.35 ns. After reacting with TYR and phenol, the average lifetime of APBA-$CuInS_2$ QDs was 22.01 ns, containing 0.43 ns (37.28%), 4.73 ns (27.66%) and 58.58 ns (35.07%). The lifetimes of APBA-$CuInS_2$ QDs nearly had no change after adding phenol and TYR,

indicating the fluorescence quenching of APBA-$CuInS_2$ QDs belongs to the static quenching mechanism. That is, the product (catechol) of TYR and phenol adsorbed onto the APBA-$CuInS_2$ QDs surface and formed stable boronate complexes to induce the fluorescence quench.

To further validated the feasibility of sensing system for phenol and TYR detection, the fluorescence emission spectra of APBA-$CuInS_2$ QDs, APBA-$CuInS_2$ QDs/TYR, APBA-$CuInS_2$ QDs/phenol and APBA-$CuInS_2$ QDs /phenol/TYR were shown in **Fig. S4**. It can be observed that the photoluminescence (PL) at 736 nm would not be influenced by phenol (25 μmol L^{-1}) or TYR (5 U mL^{-1}) separately. When 25 μmol L^{-1} phenol and 5 U mL^{-1} TYR were both existed in the system, the PL intensity of APBA-$CuInS_2$ QDs were quenched nearly 83%. In the view of the above results, the proposed method could detect phenol and TYR based on the fluorescence quenching of APBA-$CuInS_2$ QDs.

3.3. Optimization of the sensing procedure

The sensitivity of the proposal biosensor is related to many factors, such as the pH of solution, the incubation time and the reaction temperature, so the experimental conditions are optimized for determination of phenol and TYR activity. The effect of pH on the PL intensity ratio $(F_0\text{-}F)/F_0$ of APBA-$CuInS_2$ QDs/TYR system in the presence of 20 μmol L^{-1} phenol was studied in **Fig. S5A**. F_0 and F were the PL intensity of the APBA-$CuInS_2$ QDs/TYR system in the absence and presence of phenol, respectively. When the pH value changed from 5.8 to 7.4, the PL intensity ratio of APBA-$CuInS_2$ QDs solution gradually increased. Then the remarkable decreasing of the PL intensity ratio was observed in the pH range of 7.8–8.6. The high pH value was favorable for the interaction of boronic acid and catechol, because the formation of boronate complexes was a release proton reaction. However, the electrostatic repulsion among APBA-$CuInS_2$ QDs increased

at higher pH value which further hinders the assembly of APBA-$CuInS_2$ QDs, resulting in the decreased quenching efficiencies. In addition, the PL intensity ratio gives the best result for the determination of phenol at pH 7.4. Considering the above results, pH 7.4 Tris-HCl buffer (10 mmol L^{-1}) was chosen as the optimal pH for phenol detection. Reaction time was also an important factor which had significant influence on the PL intensity ratio, therefore the time optimization was investigated in the in the Tris-HCl buffer (pH 7.4) at 37 ℃. The result in **Fig. S5B** showed that PL intensity ratio of APBA-$CuInS_2$ QDs system increased immediately after the addition of phenol and reached a balance in 60 min, which indicated the oxidation of phenol and the formation of boronate complexes completed within 60 min. Thus, the optimal incubation time was chosen 60 min.

We also investigated the effect of temperature on the PL intensity ratio of APBA-$CuInS_2$ QDs/TYR/phenol system. The temperature adopted in this study was 4, 15, 30, 37 and 45 ^{o}C. As shown in **Fig. S5C**, The PL intensity ratio of APBA-$CuInS_2$ QDs/TYR/phenol system gradually increased with the increasing temperature and reached the highest at 37 ^{o}C. When the temperature increased to 45 ^{o}C, the PL intensity ratio decreased again. The results indicated that the temperature had a close relationship with TYR activity. If the temperature was too high or too low, TYR can have conformational changes and be inactivation during the oxidation process. Regarding above results, we chose 37 ^{o}C as the optimal reaction temperature for phenol and ACP detection in the further experiments, which was consistent with the optimum temperature of the catalytic behavior of TYR.

3.4. Determination of phenol and enzyme activity

The determination of phenol and TYR activity with the above biosensor was conducted under

the optimum conditions. As shown in **Fig. 2A**, the PL intensity of APBA-$CuInS_2$ QDs decreased gradually with the increasing concentration of phenol. **Fig. 2A** inset illustrated there was a good linear relationship between the PL intensity ratios $(F_0\text{-}F)/F_0$ of APBA-$CuInS_2$ QDs/TYR system and the concentration of phenol in the range from 0.25 to 25 μmol L^{-1}. F_0 and F were the PL intensity of the APBA-$CuInS_2$ QDs/TYR system in the absence and presence of phenol, respectively. The regression equation is: $(F_0\text{-}F)/F_0$ =0.05624 + 0.03143 [phenol], μmol L^{-1}. The corresponding regression coefficient is 0.994. The limit of detection (LOD) was calculated to be 0.05 μmol L^{-1}, this value is comparable to those of previously reported methods (**Table S2**), which suggests that the proposed biosensor is efficient for phenol detection. According to previous literature, the European Union established maximum allowable total and individual phenol concentrations in water for human consumption of 0.5 mg L^{-1} (~5 μmol L^{-1}) and 0.1 mg L^{-1} (~1 μmol L^{-1}), respectively (Zeng et al., 2015). Thus our proposed methods could satisfy the requirements for phenol detection in water sample.

In addition, we also studied the interaction between phenol and $CuInS_2$ QDs in the presence of TYR. From **Fig. 2B**, it can be observed that the PL intensity of $CuInS_2$ QDs at 660 nm was also decreased with the increasing concentration of phenol in the range of 5-25 μmol L^{-1}. As we know, TYR can catalyze the hydroxylation of phenol substrates to catechol, further oxidised to o-quinone (Chang et al., 2009). o-quinone, which could accept the electron, was reported as a fluorescence quencher (Canbay et al., 2014; Zhu et al., 2015). So the PL intensity of $CuInS_2$ QDs/TYR system could be quenched by adding phenol. A liner relationship between the PL intensity ratios $(F_0\text{-}F)/F_0$ of $CuInS_2$ QDs/TYR and the concentration of phenol were shown in the inset of **Fig. 2B**. The regression equation is: $(F_0\text{-}F)/F_0$ = 0.00529 + 0.00544 [phenol], μmol L^{-1}. The corresponding

regression coefficient (R^2) is 0.991, and LOD for phenol is 1.8 μmol L^{-1}. According to above performance, the APBA-$CuInS_2$ QDs/TYR system had the lower detection limit and the higher sensitivity for phenol detection by comparison with $CuInS_2$ QDs/TYR system. It is because the boronic acid functional groups were reactive toward catechol to form five-member cyclic boronate esters at the surface of $CuInS_2$ QDs. So the distance between boronate esters and $CuInS_2$ QDs are much closer than that of o-quinone and $CuInS_2$ QDs, leading to more efficient quenching of fluorescence. It could be concluded that the presence of APBA could improve the sensitivity of sensing system for phenol detection.

This method can also be applied to TYR detection. APBA-$CuInS_2$ QDs were mixed with 25 μmol L^{-1} of phenol and different concentrations of TYR for 60 min incubating at 37 °C. As describe in **Fig. 2C**, in the range from 0.1 U mL^{-1} to 10 U mL^{-1}, the PL intensity ratios $(F_0\text{-}F)/F_0$ of APBA-$CuInS_2$ QDs exhibit an excellent linear relationship to the concentration of TYR (R^2=0.995), and the detection limit of TYR is 0.03 U mL^{-1}. What's more, a comparison between our method and other reported methods for TYR detection in linear range and LOD were summed up in **Table S3**. Compared with other sensing methods, the sensitivity of this proposed NIR fluorescent biosensor was comparable to that of previously reported sensing systems.

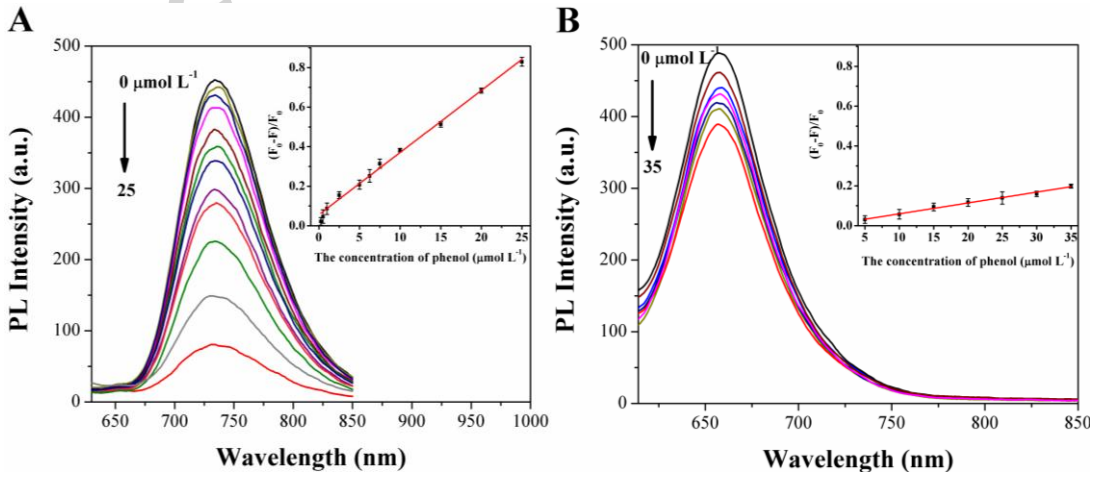

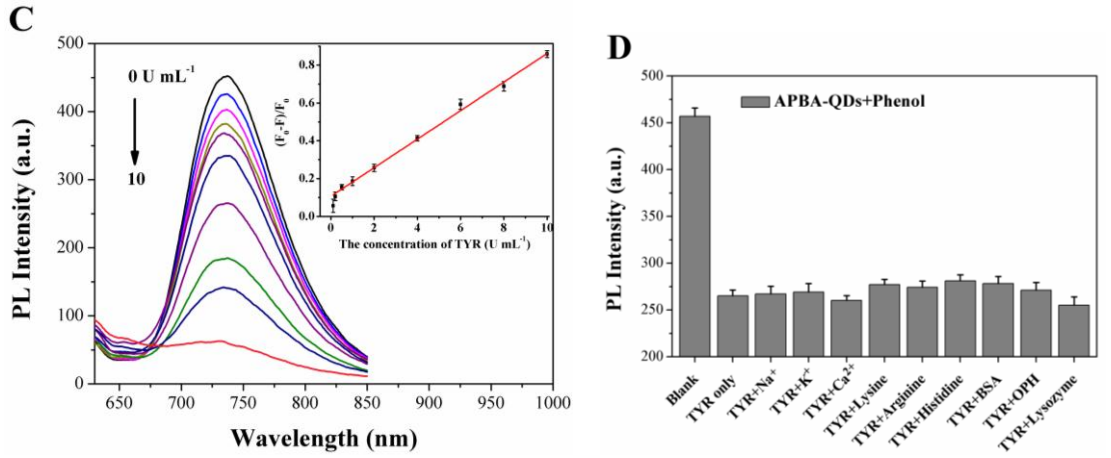

Fig. 2 (A) The fluorescence spectra of APBA-$CuInS_2$ QDs/TYR system in the presence of different concentration of phenol (0, 0.25, 0.5, 1.0, 2.5, 5.0, 6.25, 7.5, 10, 15, 20 and 25 μmol L^{-1}). Inset: the PL intensity ratio $(F_0\text{-}F)/F_0$ of versus the concentration of phenol. (B) The fluorescence spectra of $CuInS_2$ QDs/TYR system in the presence of different concentration of phenol (0, 5.0, 10, 15, 20 and 25 μmol L^{-1}). Inset: the PL intensity ratio $(F_0\text{-}F)/F_0$ of versus the concentration of phenol. (C) The fluorescence spectra of APBA-$CuInS_2$ QDs/phenol system in the presence of different concentration of TYR (0, 0.1, 0.2, 0.4, 1.0, 2.0, 4.0, 6.0, 8.0 and 10.0 U mL^{-1}). Inset: the PL intensity ratio $(F_0\text{-}F)/F_0$ of versus the concentration of TYR. All the RSD values were less than 3.5% (values are mean of three replicates). (D) Fluorescence response of APBA-$CuInS_2$ QDs/phenol to TYR (4 U mL^{-1}) or the mixture of the coexisting substances with TYR.

Phenol-induced fluorescence turn-off of APBA-$CuInS_2$ QDs/TYR is suited to detect the activity of hydrolases and their substrates, such as PP could be rapidly hydrolyzed to generate phenol by ACP. To test this hypothesis, APBA-$CuInS_2$ QDs were used to quantitatively detect ACP in the presence of PP. Here we studied the interaction between ACP, PP and $CuInS_2$ QDs. As shown in **Fig. S6A–B**, ACP and PP also have no remarkable influence to the PL intensity of APBA-$CuInS_2$ QDs/TYR system, which indicated the interaction between PP, ACP and

APBA-$CuInS_2$ QDs could be ignored. However, the PL quenching could be observed obviously with the simultaneous addition of ACP and PP into the sensing system (**Fig. S6C**). As the ACP concentration increased at a fixed PP concentration, the fluorescence of APBA-$CuInS_2$ QDs at 736 nm gradually decreased. On plotting the PL intensity ratios $(F_0\text{-}F)/F_0$ against the ACP concentration, a linear relationship (R^2=0.995) for ACP quantification was observed in the range 25-2250 nU mL^{-1} (**Fig. 3A**), and the detection limit of ACP is 6.2 nU mL^{-1}. It presented a comparable sensitivity comparing with other reported detection methods for ACP activity (**Table S4**). The successful probing of ACP suggested the implementation of APBA-$CuInS_2$ QDs for detecting other enzymes and their substrates.

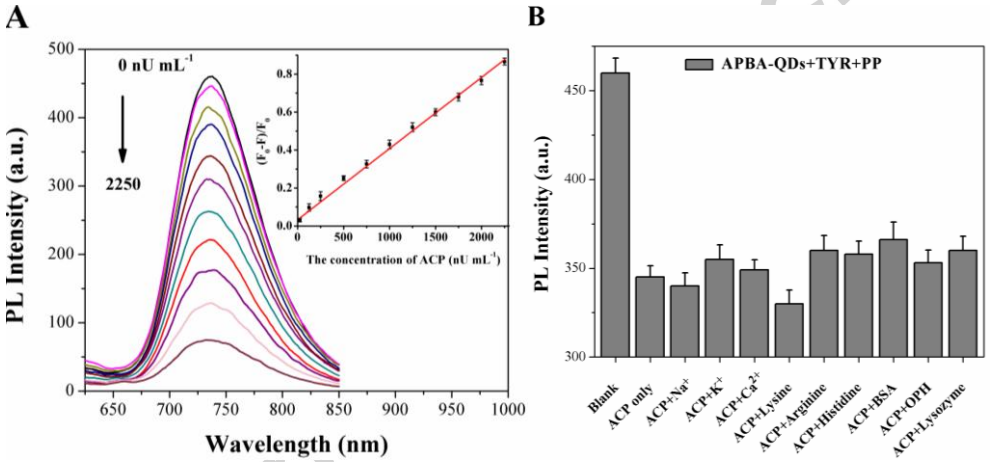

Fig. 3 (A) The fluorescence spectra of APBA-$CuInS_2$ QDs/TYR system in the presence of different concentration of ACP (0, 25, 125, 250, 500, 750, 1000, 1250, 1500, 1750, 2000 and 2250 nU mL^{-1}). Inset: the PL intensity ratio $(F_0\text{-}F)/F_0$ of versus the concentration of ACP. The RSD values were less than 2.4% (values are mean of three replicates). (B) Fluorescence response of APBA-$CuInS_2$ QDs/TYR/PP to ACP (500 nU mL^{-1}) or the mixture of the coexisting substances with ACP.

3.5. Selectivity for phenol and enzyme

Selectivity is a very important parameter to evaluate the performance of a new fluorescence biosensor. Thus, the selectivity of the proposed method was further investigated with various coexistence substances added. As shown in **Fig. S7,** the tolerable concentration ratios of coexisting substances to 10 μmol L^{-1} phenol was 10-fold for K^+, Na^+, Ca^{2+}, Ba^{2+}, Zn^{2+}, Mg^{2+}, Fe^{2+}, Cu^{2+}, Fe^{3+}, lysine, arginine, histidine, p-phenylenediamine, p-aminobenzenesulfonate, o-nitroaniline, 1,4-dimethyl-benzene, phenyl phosphate and 1-chloro-4-nitrobenzene. It can be seen that the PL intensity of APBA-$CuInS_2$ QDs/TYR system in absence and presence of phenol have no obvious change, which indicates that the common inorganic ion, amine acids and phenol derivatives do not have evident interference on phenol detection. It was also observed that 20 μg mL^{-1} K^+, Na^+, Ca^{2+}, lysine, arginine, histidine, bovine serum albumin (BSA), organophosphorus hydrolase (OPH) and lysozyme had no effective influence to our detection of TYR activity (**Fig. 2D).** This good selectivity of APBA-$CuInS_2$ QDs/TYR biosensor might be due to the strong affinity of boronic acid group to catechol and the special catalyzation of TYR. **Fig. 3B** showed that 20 μg mL^{-1} K^+, Na^+, Ca^{2+}, lysine, arginine, histidine, BSA, OPH and lysozyme had no obvious influence to APBA-$CuInS_2$ QDs/TYR/PP system in the presence of 500 nU mL^{-1} (~2×10^{-4} μg mL^{-1}) ACP. These results showed that there was little interference from commonly existing substances. Thus, the present method was suitable for selective detection of phenol, TYR and ACP.

3.6. Real samples detection

Given its extreme toxicity, phenol presence in the environment poses toxic risks to human health and may result in drastic ecological problem (Alkasir et al., 2012). So the developed fluorescence biosensor was applied for the determination of phenol in environmental samples, such as tap water, river water and mineral water. The average recovery test was made by using the

standard addition method. The analytical results were listed in **Table 1**. It can be seen that the relative standard deviation (RSD) was lower than 4.03% and the average recoveries of phenol in real samples were in the range of 90–107%, indicating that the accuracy and precision of the proposed method were satisfactory. The above results demonstrated the potential applicability of the APBA-$CuInS_2$ QDs/TYR based fluorescence biosensor for the phenol detection in environmental samples.

Table 1 Detection of phenol in environmental samples

Sample	Original found (μmol L^{-1})	Spiked concentration (μmol L^{-1})	Found phenol (μmol L^{-1})	Recovery (%)	RSD (n=3, %)
Tap water	0	0	/	/	/
	0	0.50	0.50	98	1.03
	0	1.00	1.03	103	2.84
	0	5.00	5.34	107	2.57
River water	0	0	/	/	/
	0	0.50	0.45	90	4.03
	0	1.00	0.97	97	3.77
	0	5.00	5.02	100	2.95
Mineral water	0	0	/	/	/
	0	0.50	0.48	95	2.43
	0	1.00	0.92	92	3.93
	0	5.00	4.79	96	3.00

3.7. In vitro TYR sensing

In order to assess the intracellular localization of the endocytosed APBA-$CuInS_2$ QDs, human prostate cancer cells (PC-3M) were incubated with APBA-$CuInS_2$ QDs. The PC-3M cultured in the medium without glucose was chosen as model samples. As shown in **Fig. S8**, APBA-$CuInS_2$ QDs were easily found in cytoplasm with good dispersivity. This result implied that APBA-$CuInS_2$ QDs can be used as a biocompatible probe *in vitro* imaging. Having demonstrated the

effectiveness of APBA-$CuInS_2$ QDs/phenol system in sensing TYR producing a "turn off" fluorescence signal, we further used the proposed biosensors for intracellular TYR specific imaging in PC-3M cells. The PC-3M cells were incubated with 0, 1.0 and 5.0 U mL^{-1} TYR for 3 h in IMDM medium supplemented with 10% fetal bovine serum at 37 ^{0}C, and washed with PBS buffer (pH 7.4) to remove any free TYR from the ACP-uptaken cells. Then, the treated PC-3M cells were incubated under the condition of serum starvation with APBA-$CuInS_2$ QDs/phenol for 60 min until the reaction between TYR and APBA-$CuInS_2$ QDs/phenol finished. Finally, fluorescent photos of the cells were recorded and analyzed by fluorescence microscopy. The fluorescence microscopic photograph presented in **Fig. 4A** shows that a strong intracellular fluorescence was observed throughout the cells. In contrast, there is a significant decrease in the intracellular fluorescence in the TYR (1.0 U mL^{-1})-uptaken PC-3M cells with APBA-$CuInS_2$ QDs/phenol (**Fig. 4B**). Furthermore, the cells exposed to 5.0 U mL^{-1} of TYR displayed weaker red fluorescence (**Fig. 4C**) than those exposed to 1.0 U mL^{-1} of TYR. The corresponding fluorescence color change in **Fig. 4** clearly indicated that the high sensitivity of the APBA-$CuInS_2$ QDs/phenol probe can serve as a potential biocompatible nanoprobe for TYR activity detection in the intracellular region.

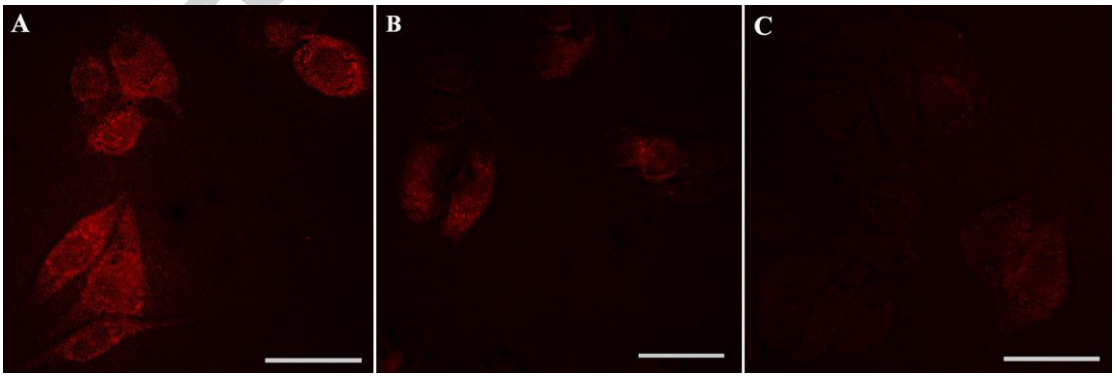

Fig. 4 The fluorescent microscopy images of PC-3M cells counterstained with (A) 0 U mL^{-1}, (B) 1.0 U mL^{-1} and (C) 5.0 U mL^{-1} TYR for 3 h, followed by further incubation with APBA-$CuInS_2$

QDs/phenol probe for 60 min. The concentration of phenol was 5 μmol L^{-1}. The scale bar in the fluorescence images is 10 μm.

4. Conclusion

In conclusion, we have successfully developed a novel NIR fluorescence biosensor for phenol and enzyme activity detection by employing APBA-$CuInS_2$ QDs. Phenyl phosphate could be rapidly hydrolyzed to phenol via the ACP-catalyzed reaction. The reaction of TYR and phenol could form catechol, and the phenylboronic acid of the functionalized $CuInS_2$ QDs would form boronate esters with catechol which produce the quenched fluorescence signal. Utilizing the variation of fluorescence intensity, a simple, sensitive and selective sensing method for phenol, TYR and ACP activity were constructed with the detection limits of 0.05 μmol L^{-1}, 0.03 U mL^{-1} and 6.2 nU mL^{-1}, respectively. Using the fluorescence probe, we successfully performed an *in vitro* imaging of human prostate cancer cells. Comparing with previously reported phenol and enzyme activity probing strategy, the proposed biosensor is simple, facile, and has a higher sensitivity and better selectivity. All these results obviously indicated that the implementation of APBA-$CuInS_2$ QDs for detecting enzymes and their substrates.

Acknowledgments

We greatly appreciate the support of the National Natural Science Foundation of China (Nos. 21075050, No. 21275063) the Science and Technology Development Project of Jilin Province, China (No. 20150204010GX) and Graduate Innovation Fund of Jilin University (No. 2015022).

References

Alkasir, R.S.J., Ornatska, M., Andreescu, S., 2012. Anal. Chem. 84, 9729−9737.

1 Azmi, N.E., Ramli, N.I., Abdullah, J., Hamid, M.A.A., Sidek, H., Rahman, S.A., Ariffin, N., Yusof,
2 N.A., 2015. Biosens. Bioelectron. 67, 129–133.
3 Breger, J.C., Sapsford, K.E., Ganek, J., Susumu, K., Stewart, M.H., Medintz, I.L., 2014. ACS Appl.
4 Mater. Interfaces, 6, 11529−11535.
5 Canbay, E., Akyilmaz, E., 2014. Anal. Biochem. 444, 8–15.
6 Chang, T.S., 2009. Int. J. Mol. Sci. 10, 2440–2475.
7 Chen, G., Song, F., Xiong, X., Peng, X., 2013. Ind. Eng. Chem. Res. 52, 11228−11245.
8 Derfus, A.M., Chan, W.C., Bhatia, S.N., 2004. Nano lett. 4, 11−18.
9 Freeman, R., Girsh, J., Willner, I., 2013. ACS Appl. Mater. Interfaces 5, 2815−2834.
10 Gao, X., Tang, G.C., Su, X.G., 2012. Biosens. Bioelectron. 36, 75–80.
11 Gill, R., Freeman, R., Xu, J., Willner, I., Winograd, S., Shweky, I., Banin, U., 2006. J. Am. Chem.
12 Soc. 128, 15376–15377.
13 Gill, R., Zayats, M., Willner, I., 2008. Angew. Chem. Int. Ed. 47, 7602−7625.
14 Hoshino, A., Fujioka, K., Oku, T., Suga, M., Sasaki, Y.F., Ohta, T., Yasuhara, M., Suzuki, K.,
15 Yamamoto, K., 2004. Nano Lett. 4, 2163–2169.
16 Jin, T., Fujii, F., Yamada, E., Nodasaka, Y., Kinjo, Masataka, 2006. J. Am. Chem. Soc. 128,
17 9288–9289.
18 Kirchner, C., Liedl, T., Kudera, S., Pellegrino, T., Muñoz Javier, A., Gaub, H. E., Stolzle, S., Fertig,
19 N., Parak, W. J., 2005. Nano Lett. 5, 331−338.
20 Li, L., Wu, P., Wang, K.H., Lu, Y., 2013. J. Am. Chem. Soc. 135, 2411−2414.
21 Liu, S.Y., Shi, F.P., Zhao, X.J., Chen, L., Su, X.G., 2013. Biosens. Bioelectron. 47, 379–384.
22 Liu, S.Y., Su, X.G., 2014. RSC Adv. 4, 43415–43428.

1 Lin, Z.H., Ma, Q., Fei, X.F., Zhang, H., Su, X.G., 2014. Anal. Chim. Acta 818, 54–60.

2 Medintz, I.L., Uyeda, H.T., Goldman, E.R., Mattoussi, H., 2005. Nat. Mater. 4, 435−446.

3 Meng, X.W., Wei, J.F., Ren, X.L., Ren, J., Tang, F.Q., 2013. Biosens. Bioelectron. 47, 402−407.

4 Morris-Cohen, A.J., Malicki, M., Peterson, M.D., Slavin, J.W.J., Weiss, M.A., 2013. Chem. Mater.

5 25, 1155−1165.

6 Pradhan, N., Peng, X.G., 2007. J. Am. Chem. Soc. 129, 3339–3347.

7 Qu, Z.B., Zhou, X.G., Gu, L., Lan, R.M., Sun, D.D., Yu, D.J., Shi, G.Y., 2013. Chem. Commun. 49,

8 9830–9832.

9 Serrano, I.C., Stoica, G., Adams, A.M., Palomares, E., 2014. Nanoscale, 6, 13623-13629.

10 Tang, B., Cao, L.H., Xu, K.H., Zhuo, L.H., Ge, J.C., Li, Q.L., Yu, L.J., 2008. Chem. Eur. J. 14,

11 3637–3644.

12 Tang, Y., Yang, Q., Wu, T., Liu, L., Ding, Y., Yu, B., 2014. Langmuir 30, 6324−6330.

13 Van Veggel F.C.J.M., 2013. Chem. Mater. 26, 111–122.

14 Van Dyk, J. S., Pletschke, B., 2011. Chemosphere 82, 291–307.

15 Wu, P., Yan, X. P., 2013. Chem. Soc. Rev. 42, 5489−5521.

16 Wu, W.T., Zhou, T., Berliner, A., Banerjee, P., Zhou, S.Q., 2010. Angew. Chem., Int. Ed. 49,

17 6554–6558.

18 Xia, Y.S., Song, L., Zhu, C.Q., 2011. Anal. Chem. 83, 1401–1407.

19 Yong, K.T., Roy, I., .Ding, H., Bergey, E.J., Prasad, P.N., 2009. Small 5, 1997–2004.

20 Yan, X., Li, H.X., Han, X.S., Su, X.G., 2015a. Biosens. Bioelectron. 74, 277–283.

21 Yan, X., Li, H.X., Zheng, W.S., Su, X.G., 2015b. Anal. Chem. 87, 8904–8909.

22 Zeng, Z.M., Tian, L.J., Li, Z., Jia, L., Zhang, X.Y., Xia, M.M., Hu, Y.G., 2015. Biosens.

Bioelectron. 69, 162–166.

Zhu, X.L., Hu, J., Zhao, Z.H., Sun, M.J., Chi, X.Q., Wang X.M., Gao, J.H., 2015. Small 11, 862–870.

Highlights:

► A novel and convenient fluorescence nanosensor for detection of phenol and tyrosinase was established.

► The functionalized $CuInS_2$ QDs have a fairly symmetric fluorescence emission in the near-infrared spectral region.

► The biosensing platform could also sensitively detect the phenol product-related enzyme system.

► The fluorescence probe can serve as a biocompatible nanoprobe for tyrosinase detection in the intracellular region.